



HAL
open science

On the implications of nitromethane – NO chemistry interactions for combustion processes

Krishna Prasad Shrestha, Lars Seidel, Thomas Zeuch, Gladys Moréac,
Philippe Dagaut, Fabian Mauss

► **To cite this version:**

Krishna Prasad Shrestha, Lars Seidel, Thomas Zeuch, Gladys Moréac, Philippe Dagaut, et al.. On the implications of nitromethane – NO chemistry interactions for combustion processes. *Fuel*, 2021, 289, pp.119861. 10.1016/j.fuel.2020.119861 . hal-03115005

HAL Id: hal-03115005

<https://hal.science/hal-03115005>

Submitted on 19 Jan 2021

HAL is a multi-disciplinary open access archive for the deposit and dissemination of scientific research documents, whether they are published or not. The documents may come from teaching and research institutions in France or abroad, or from public or private research centers.

L'archive ouverte pluridisciplinaire **HAL**, est destinée au dépôt et à la diffusion de documents scientifiques de niveau recherche, publiés ou non, émanant des établissements d'enseignement et de recherche français ou étrangers, des laboratoires publics ou privés.

Copyright

On the implications of nitromethane - NO_x chemistry interactions for combustion processes

Krishna Prasad Shrestha^{1, *}, Lars Seidel², Thomas Zeuch³, Gladys Moréac^{4, 5}, Philippe Dagaut⁵,
and Fabian Mauss¹

1. Thermodynamics and Thermal Process Engineering, Brandenburg University of Technology, Siemens-Halske-Ring 8, 03046 Cottbus, Germany
2. LOGE Deutschland GmbH, Burger Chaussee 25, 03044 Cottbus, Germany
3. Institut für Physikalische Chemie, Georg-August-Universität Göttingen, Göttingen, Germany
4. RENAULT SAS, 78084 Guyancourt, France
5. ICARE, Centre National de la Recherche Scientifique (CNRS-INSIS), Orléans, France

*Corresponding author: Krishna Prasad Shrestha

e-mail: shrestha@b-tu.de

Abstract

In this work, we report a detailed investigation of the CH₃NO₂ chemistry effect on fuel-NO interactions for the fuels methane and *n*-heptane using a recently developed and extensively validated H₂/O₂/CO/NO_x/NH₃/CH₃NO₂ baseline chemistry. In general, the model predictions show good agreement with temperature profiles of major and intermediate species in jet-stirred reactor experiments and they capture the subtle effect of NO addition. For both fuels, the CH₃NO₂ kinetics retard the system reactivity in the low temperature range by delaying the production of key radicals like OH and HO₂. This explains the retarding effect of NO for *n*-heptane low temperature ignition and the overprediction of reactivity enhancement by NO in earlier studies on methane combustion. For methane, the recently explored roaming mediated dissociation channel of CH₃NO₂ to CH₃O + NO is a major reaction pathway for CH₃NO₂ consumption. Our analysis suggests that at higher pressure, relevant to engine conditions, the two key intermediate species HONO and CH₃NO₂ feature strongly increased concentrations during *n*-heptane combustion and they may be detectable under such conditions in combustion experiments of this fuel-NO_x system. The results of this work call for detailed future investigations of the CH₃NO₂ chemistry effect in the context of exhaust gas recirculation, also with regard to the suppression of engine knock.

Keywords: Nitromethane, NO_x, fuel-NO_x, kinetic modeling, EGR

33 1. Introduction

34 Unraveling the molecular mechanisms of complex reaction sequences is a central goal of
35 chemical research. A valid reaction mechanism gives predictive power to kinetic simulations with
36 potentially drastic implications for addressing environmental issues and industrial applications.
37 The understanding of the creation and the subsequent containment of the hole in the ozone layer
38 is perhaps the best-known example in this context [1]. Complex gas-phase reaction systems
39 govern the oxidation of hydrocarbons in the atmosphere and during combustion [2]. Missing or
40 unreliable kinetic data on single chemical steps can alter the mechanistic understanding of
41 important chemical phenomena like new particle formation in the troposphere [3] or pollutant
42 formation in flames [4]. The severe underestimation of the reaction rate of Criegee intermediates
43 (CI) with SO₂ [3] and wrong product assignments for the CH₃ + O [5] and CH + N₂ [4,6] reactions
44 in hydrocarbon flames are prominent examples of the last decades that motivate efforts in kinetic
45 research up to now [2].

46 In combustion chemistry, the understanding of NO_x formation and measures for NO_x reduction
47 in internal combustion engines are important fields of current research [7,8]. The conflict of
48 objectives in the desired reduction of both NO_x and CO₂ emissions has recently come to a political
49 crisis in the context of European clean air legislation and the growing establishment of “no drive
50 zones” even for relatively new Diesel cars. One widely applied measure for reducing NO_x in
51 Internal combustion (IC) engines is exhaust gas recirculation (EGR) which introduces preformed
52 NO to the ignition process promoting ignition and decreasing temperature and NO_x emissions
53 [9]. The enhanced auto-ignition effect has been attributed to a mutual sensitization of fuel and
54 NO oxidation [10,11]. However, the details of the underlying mechanisms and the effect of fuel
55 molecules larger than methane have not been rigorously explored so far. In the case of n-heptane
56 e.g., NO addition reduces ignitability in the low temperature range [12]. In general, the chemistry
57 of N-atom carrying radicals has gained again attention in recent years, e.g. with regard to the role
58 of NCN in NO formation [6] and ammonia as a hydrogen carrier or storage compound [13]. This
59 situation calls for developing comprehensive kinetic models that cover the now enlarged range
60 of relevant fuels and combustion conditions. To this end, we have, in a first step, compiled and
61 extensively validated an H₂/O₂/CO/NO_x mechanism, successfully extended to simulate the
62 oxidation of ammonia. The simulations have elucidated the strong influence of the HO₂ radical
63 concentrations on reducing or oxidizing NO_x conditions [14]. In our subsequent study, we
64 extended the model [14] and introduced C₁-C₂ chemistry covering hydrocarbons as well as
65 alcohols (C₁-C₂) as fuel [15]. In our most recent experimental and modeling work [16], we
66 extended our nitrogen chemistry introducing nitromethane as a fuel. Similar to our previous
67 works [14,15], the model was validated for a broad range of experimental conditions and setups
68 (speciation in jet-stirred and flow reactors and premixed flames, laminar flame speeds and
69 ignition timing). The model development approach is hierarchically in nature. In the present

70 study, this enabled a comprehensive re-examination of the ignition timing during methane and,
71 as a model system for exhaust gas recirculation in engines, *n*-heptane oxidation with premixed
72 NO_x. Very recently, significant progress has been made on the experimental side with regard to
73 the effect of NO addition. In 2018, Battin-Leclerc and co-workers [17] conducted an experimental
74 and modeling study of methane oxidation in the presence of NO_x in a jet-stirred reactor at 106.7
75 kPa. They tried to quantify the species HONO and CH₃NO₂ in their experiment but were not
76 successful in that work, concluding that these species were below the estimated detection limit
77 of 3 and 5 ppm respectively. However, in 2019 Battin-Leclerc and co-workers succeeded in
78 measuring HONO quantitatively using continuous-wave Cavity Ring-Down Spectroscopy (cw-
79 CRDS) in a follow-up study [18] on *n*-pentane oxidation in the presence of NO (500 ppm) in a jet-
80 stirred reactor at 106.7 kPa under stoichiometric conditions. The determined peak concentration
81 of HONO was 256 ppm (± 24 ppm); however, the detection of CH₃NO₂ was not reported. This is
82 clearly an important step in improving our understanding of the specific low-temperature
83 oxidation chemistry of fuel – NO_x systems and the question arises if there are conditions under
84 which CH₃NO₂ can be detected. In this study, we make use of the recent progress in characterizing
85 chemical NO_x/CH₃NO₂ fuel interactions for a detailed kinetic modelling study of the mechanism
86 of the exhaust gas recirculation effect, augmenting the experimental target range by jet stirred
87 reactor experiments on *n*-heptane oxidation in the presence of NO. The ensuing analysis
88 illustrates the crucial role of nitromethane chemistry for this important industrial application and
89 identifies experimental conditions under which an *in-situ* detection of CH₃NO₂ may be achieved.

90 **2. Kinetic Model**

91 The complete nitromethane/NO_x kinetic model used in this work comes from our recently
92 published work Shrestha et. al. [16] which was built hierarchically and validated for a wide range
93 of experimental conditions (speciation in a jet-stirred and flow reactor, speciation in premixed
94 flames, laminar flame speeds and ignition delay times). In this recent study [16] the roaming
95 isomerization path of nitromethane was introduced, where nitromethane can isomerize to
96 methyl nitrate (CH₃ONO) finally dissociating to CH₃O+NO (CH₃NO₂→CH₃ONO→CH₃O+NO). The
97 importance of this path was not shown in previously published literature models. A detailed
98 description of this pathway can be found in our recent work [16].

99 In the present work, two fuels are investigated namely methane (CH₄) and *n*-heptane (*n*-C₇H₁₆).
100 For methane oxidation, our recently published kinetic model [16] is used which was validated
101 broadly (speciation in a jet-stirred and flow reactor, speciation in premixed flames, laminar flame
102 speeds and ignition delay times) for H₂, NH₃, C₁-C₂ fuels including NO_x chemistry which can be
103 found in our previous study Shrestha et. al. [14,15]. The *n*-heptane kinetic scheme used in this
104 study is taken from a previous experimental and modeling study (Seidel et. al. [19]) with a focus
105 on *n*-heptane flame chemistry. The *n*-heptane mechanism was also validated in a multi setup
106 experiment using literature data (see [19] for *n*-heptane model validation).

107 To describe the oxidation of *n*-heptane/NO_x blends and the impact of nitromethane kinetics, the
108 complete nitrogen chemistry (which also includes nitromethane) from [16] is coupled with the *n*-
109 heptane kinetic scheme from Seidel et al. [19]. The thermochemistry data and transport
110 properties of the species are also taken from [16] and [19]. The complete *n*-heptane/nitrogen
111 chemistry model consists of 402 species and 2543 reversible reactions which is provided in the
112 supplementary material (SM).

113 **2.1 Brief overview of nitromethane decomposition**

114 Since this study demonstrates the importance of the CH₃NO₂ chemistry during fuel/NO_x
115 interaction, before moving ahead we will discuss briefly on CH₃NO₂ decomposition chemistry.

116 During the fuel oxidation in presence of NO_x nitromethane is mainly formed through the
117 recombination of CH₃ and NO₂ [15,20]. Nitromethane itself as a fuel can undergo thermal
118 decomposition to form CH₃ and NO₂ [16]. However, several recent studies [21–25] on the thermal
119 decomposition of CH₃NO₂ suggest that CH₃NO₂ not only thermally dissociates to CH₃+NO₂, but
120 can also isomerize to methyl nitrate (CH₃ONO) *via* a roaming type transition state finally
121 dissociating to CH₃O+NO. Zhu and Lin [21] studied the CH₃NO₂ decomposition theoretically and
122 suggested that the channel to CH₃O+NO could be detected in experiments. The theoretical
123 analysis by Annesley et al. [24] suggests that at pressures above 2 Torr the product distribution
124 undergoes a sharp transition from the roaming dominated (CH₃ONO → CH₃O+NO) to the bond-
125 fission dominated (CH₃+NO₂) channel. Hence the bond fission channel is dominating for
126 combustion environments featuring significantly higher pressures in agreement with the studies
127 mentioned above. Furthermore, this finding is supported by the later study of Matsugi and Shiina
128 [25] who proposed branching ratios of 0.97 and 0.03 in favor of the C-N bond fission channel
129 (CH₃+NO₂). Despite its low branching ratio of the CH₃O+NO channel, it is clearly recommended
130 to take into account the roaming type channel in kinetic modeling studies [26].

131 Nitromethane can also undergo decomposition through secondary reaction channels: it can react
132 with H atoms to yield CH₃+HNO₂, CH₃NO+OH, and CH₂NO₂+H₂. CH₃NO₂ can also react with OH
133 radicals to form CH₂NO₂+H₂O or CH₃OH+NO₂. Furthermore, CH₃NO₂ can undergo H abstraction
134 reacting with radicals such as O, HO₂, O₂, NO₂, CH₂-3, CH₂-1, CH₃, CH₃O, and C₂H₅ mainly forming
135 CH₂NO₂ and the related products. The detailed discussion on the adopted rate parameters for
136 the decomposition channels of nitromethane can be found in our previous work [15,16].

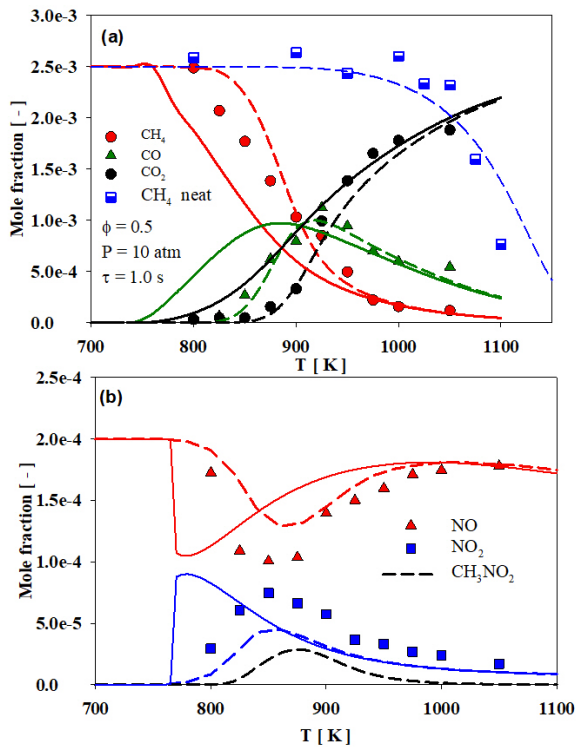
137 **3. Results and Discussion**

138 In all the figures shown below the solid lines represent the predictions without nitromethane
139 chemistry and the dashed lines represent those with nitromethane chemistry unless stated
140 differently. The symbols in the figures are the experimental data from our previous work [10–
141 12]. All the simulations are performed with LOGEresearch v1.10 [27].

142

143 **3.1. Effect of CH₃NO₂ kinetics on CH₄ oxidation in the presence of NO**

144 In Fig. 1 the results of an experiment under fuel-lean conditions ($\phi=0.5$) for 2.5% CH₄ and 1 % O₂
 145 in nitrogen are shown for neat CH₄ and with 200 ppm NO added [10]. These jet-stirred reactor
 146 experiments are simulated using a perfectly stirred reactor model. In the upper panel (Fig. 1a)
 147 the steady-state concentrations of the methane, CO, and CO₂ are plotted as a function of reactor
 148 temperature (symbols) and compared to simulations with two versions of the here presented
 149 model, one with (dashed line) and one without (solid line) the CH₃NO₂ sub-mechanism. The
 150 comparison reveals that the model without CH₃NO₂ chemistry is incomplete and unable to
 151 predict the onset temperature for fuel conversion and the breadth of the temperature range
 152 from beginning to almost complete fuel conversion. This problem carries through to the CO and
 153 CO₂ profiles, which follow the too early onset of fuel conversion. A similar result was obtained in
 154 the kinetic modeling study of [10], which did not include nitromethane chemistry. In contrast,
 155 the simulation including the nitromethane sub-mechanism closely follows the experimental
 156 traces of CH₄, CO, and CO₂ with deviations that are within the experimental errors. We have
 157 investigated this strong effect of nitromethane kinetics on fuel oxidation in the presence of NO
 158 utilizing flow and sensitivity analysis.



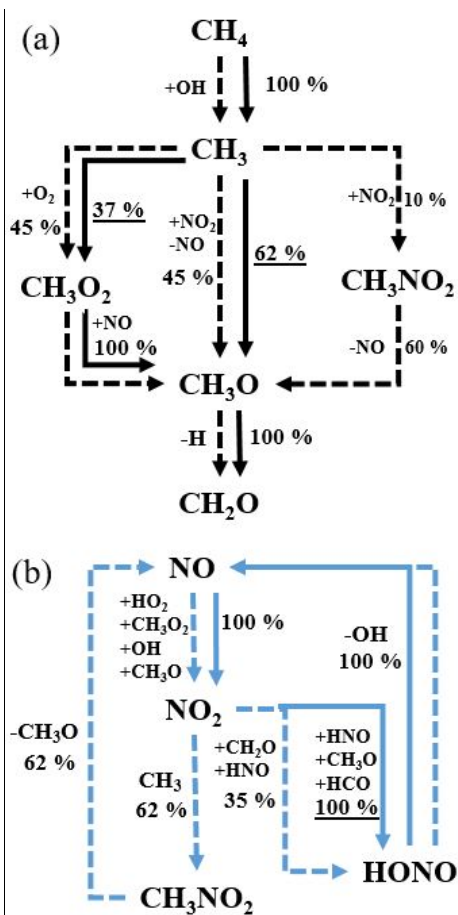
159
 160 **Figure 1:** Oxidation of CH₄/O₂/N₂ doped with 200 ppm NO and without NO in JSR at 10 atm, $\phi =$
 161 0.5, and $\tau = 1.0$ s. Symbols: measurements from Dagaut et al. [10], filled symbols: measurements

162 in the presence of NO, open symbols: measurements without NO. Solid lines: predictions without
163 CH₃NO₂ chemistry, dashed lines: predictions with CH₃NO₂ chemistry [16].

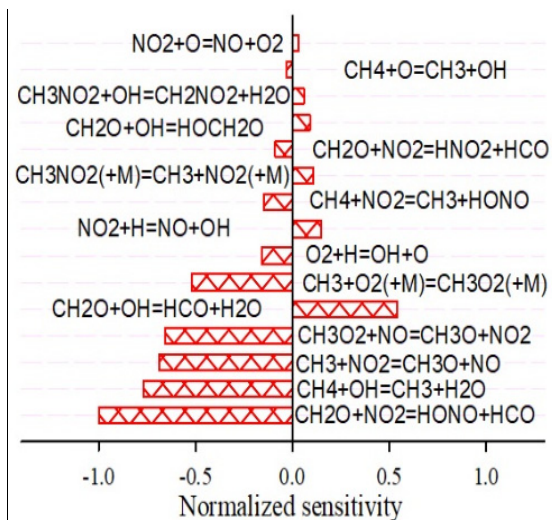
164 Figure 2 shows the integrated mass flux analysis based on C-atoms (a) and based on N-atoms (b)
165 at 840 K for the condition shown in Fig. 1 in presence of 200 ppm of NO, solid lines (without
166 CH₃NO₂ chemistry), and dashed lines (with CH₃NO₂ chemistry). It can be observed in Figure 2(a)
167 that CH₄ is completely decomposed to CH₃ by reacting with OH radicals in both cases. In line with
168 the sensitivity analysis (shown in Fig. 3), it is the second most sensitive reaction. It can be
169 observed that without CH₃NO₂ chemistry the formed CH₃ completely goes to CH₃O₂ (37 %) and
170 CH₃O (62 %) *via* reactions CH₃O₂ (+M) =CH₃+O₂ (+M) and CH₃+NO₂=CH₃O+NO respectively. The
171 latter reaction is the main consumption path of CH₃ radicals on the route to reactive NO radicals.
172 The formed CH₃O₂ reacts with NO to give CH₃O and NO₂ *via* the reaction CH₃O₂+NO=CH₃O+NO₂.
173 However, in the presence of CH₃NO₂ chemistry, the mass flux analysis (Fig. 2a) reveals that CH₃
174 can also combine with NO₂ to give CH₃NO₂. In line with this observation, it can be seen in Fig. 1b
175 that the model predicts the formation of CH₃NO₂ (black dashed line) which was not measured in
176 the experiment. The formed CH₃NO₂ readily decomposes to CH₃O + NO *via* a roaming mediated
177 isomerization channel, a newly added path discussed in detail in our recent work [16]. It should
178 be noted that Battin-Leclerc and co-workers [17] included CH₃NO₂ kinetics in their model (global
179 reactions only) but they did not take into account the roaming mediated isomerization reaction
180 path [22–25]. The importance of this path was discussed in our previous work on nitromethane
181 degradation [16] and it turns out that it is even more important for the experiments analyzed in
182 this study. In the absence of this channel all of the CH₃NO₂ goes to CH₂O and HONO *via* the H
183 abstraction route (CH₃NO₂+OH=H₂O+NO+CH₂O, CH₂O+NO₂=HONO+HCO) [17], however, in our
184 case (this study) most of the CH₃NO₂ goes to CH₃O and thus recycling back NO (see Fig. 2b). This
185 gives rise to the reactivity retarding effect of nitromethane in the presence of NO (in Fig. 1) as
186 revealed by the reaction path analysis shown in Fig. 2b. It can be observed that NO reacts with
187 the radicals HO₂, CH₃O₂, OH, and CH₃O to mainly form NO₂. Without CH₃NO₂ chemistry, all of the
188 NO₂ goes to HONO reacting with HNO, CH₃O, and the HCO radical. All the formed HONO thermally
189 dissociates to give two reactive radicals NO and OH *via* the reaction NO+OH (+M) =HONO (+M)
190 increasing the reactivity of the system. However, in presence of CH₃NO₂ chemistry, most of the
191 NO₂ (62 %) reacts with CH₃ to form relatively stable CH₃NO₂ and only a minor path (35 %) goes to
192 HONO with the just outlined reactivity enhancing effect. In line with this observation is the effect
193 that the peak concentration of HONO is predicted a factor of 7 higher and significantly earlier
194 when CH₃NO₂ chemistry is not present (see Fig. 4b). Vice versa, the formation of the key radicals
195 OH and HO₂ responsible for fuel oxidation is delayed (moving towards the higher temperature)
196 when CH₃NO₂ chemistry is present (see Fig. 4a). Hence, it can be concluded that the formation
197 of nitromethane and its decomposition to CH₃O + NO retards the reactivity of the system in the
198 presence of NO_x. It should be noted that NO/NO₂ interconversion also occurs *via* the reaction of
199 NO and HO₂ radicals giving NO₂ and OH radicals and the reaction of NO₂ with H radicals reforming

200 NO and OH radicals. The OH radicals produced during the NO–NO₂ interchanging cycle interact
 201 with CH₄ promoting its conversion.

202 Furthermore, a comparison of model predictions against the recent experimental data from Song
 203 et al. [17] in the presence of NO_x (NO and NO₂) is also performed and provided in the
 204 supplementary material (Fig. S1 – S6). It is found for the NO₂ doped case (see Figure S4) that
 205 nitromethane kinetics have a similar effect as seen for the NO doped case (Figure 1). It can also
 206 be observed in Figures S1-S3 (with NO doped case) that with the increase of equivalence ratio
 207 from the lean to the rich side the effect of nitromethane kinetics on the onset of fuel oxidation
 208 is reduced significantly. This indicates that NO_x kinetics play a more important role under oxygen-
 209 rich conditions compared to the fuel-rich conditions where O₂ is consumed to form HO₂ which is
 210 subsequently converted to more reactive OH radicals [20] via the well-known reaction
 211 (NO+HO₂=NO₂+OH).

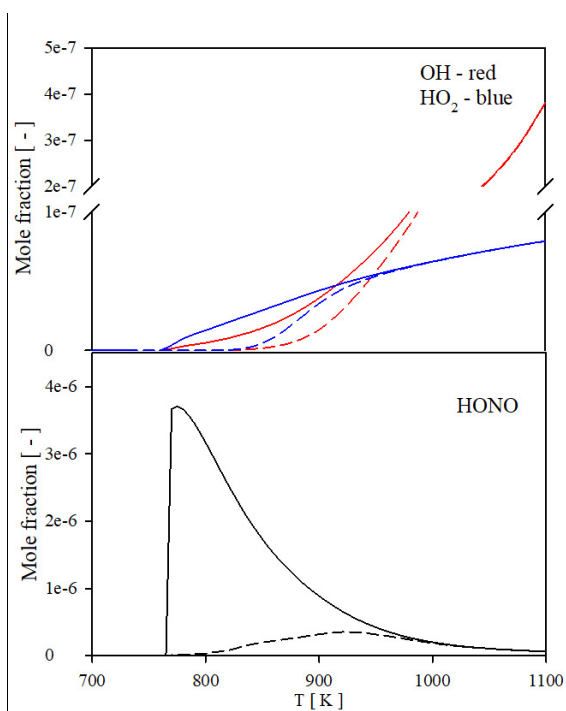


212
 213 **Figure 2:** Reaction path analysis for the condition shown in Figure 1 (doped with NO) based on C-
 214 atom (a) based on N-atom (b) at 840 K. Solid lines: without CH₃NO₂ chemistry, dashed lines: with
 215 CH₃NO₂ chemistry.



216

217 **Figure 3:** Normalized sensitivity analysis for the condition shown in Figure 1 (doped with NO) at
 218 840 K towards CH₄.



219

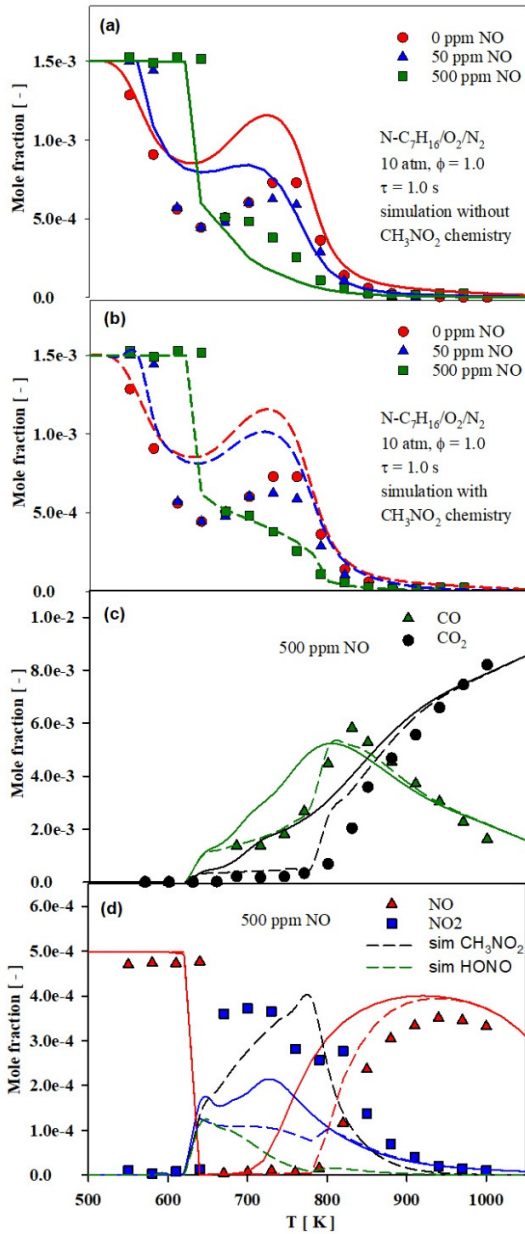
220 **Figure 4:** Predicted OH, HO₂, and HONO concentration profile with the model [16] for the
 221 condition shown in Fig. 1 (doped with NO). Dashed lines: with CH₃NO₂ chemistry; solid lines:
 222 without CH₃NO₂ chemistry.

223

224

225 **3.2 Effect of CH₃NO₂ kinetics in *n*-heptane oxidation doped with NO**

226 After elucidating the effect of nitromethane chemistry on CH₄ oxidation in the presence of NO,
 227 we investigate its effect on the larger hydrocarbon fuel *n*-heptane, which is a component of
 228 primary reference fuels and a simple model for the ignition of Diesel fuel.



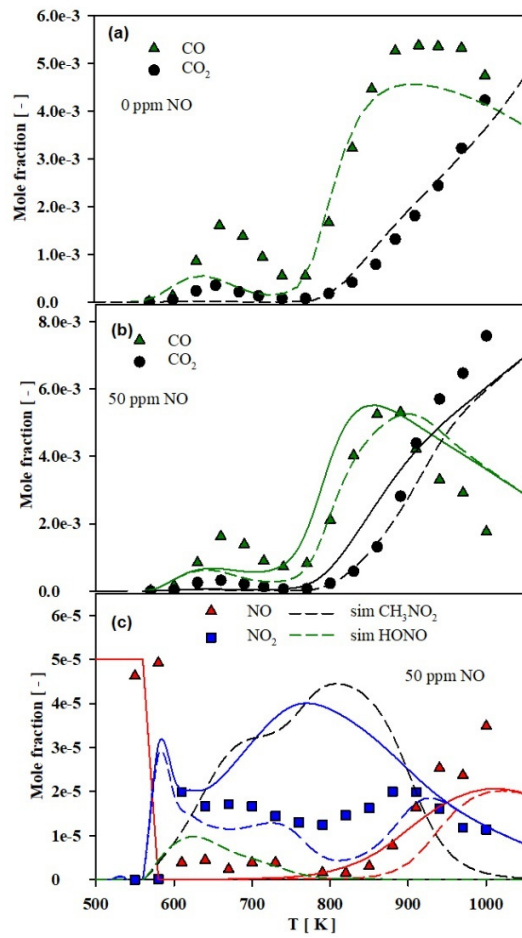
229
 230 **Figure 5:** Oxidation of *n*-C₇H₁₆/O₂/N₂ in JSR doped with and without NO at 10 atm, $\phi = 1.0$, $\tau = 1.0$
 231 s. Symbols: measurements from [12], lines: prediction with present mechanism compiled from
 232 [16,19], solid lines (without CH₃NO₂ chemistry), dashed lines (with CH₃NO₂ chemistry). *N*-heptane
 233 (*N*-C₇H₁₆) mole fraction profile (a, b); Results with 500 ppm of NO doped (c, d).

234 Figure 5 illustrates the oxidation of *n*-heptane ($n\text{-C}_7\text{H}_{16}$) in a JSR doped with 0, 50 and 500 ppm of
235 NO at 10 atm and $\tau = 1.0$ s. The experimental data are from the previous work of two of the
236 authors of this study [11,12]. Figure 5 (a, b) shows the evolution of $n\text{-C}_7\text{H}_{16}$ with temperature and
237 Figure 5 (c, d) shows the major species profile for the case doped with 500 ppm NO. For the
238 oxidation of neat *n*-heptane, the mole fraction - temperature dependence exhibits the well-
239 known behavior observed for *n*-alkanes (featuring low-temperature chemistry): a first reactivity
240 zone indicating low-temperature chemistry, a marked negative temperature coefficient area,
241 followed by a second reactivity zone corresponding to the transition to the high-temperature
242 chemistry. The temperature profiles of the fuel are quite different in the presence of the 50 and
243 500 ppm of NO. They show the ambiguous effect of NO on the oxidation of *n*-heptane: inhibition
244 of the reaction below 650 K and a reactivity enhancement above 650 K. The temperature
245 dependence still exhibits a negative temperature coefficient area, but it is much less pronounced
246 than for neat *n*-heptane. This effect has been observed earlier [12,28–31], however, in all these
247 studies the role of nitromethane chemistry in this context was not investigated. In this study, we
248 provide such an insight on nitromethane chemistry.

249 It can be observed in Fig. 5a and 5b that for the neat *n*-heptane oxidation there is, as expected,
250 no difference in $n\text{-C}_7\text{H}_{16}$ prediction with and without the CH_3NO_2 chemistry, while there are
251 significant effects when NO is present in the fuel mixture as observed in the case of methane (Fig.
252 1), especially for the 500 ppm NO case. We note that the model predictions do not exactly agree
253 with the experimental measurements for neat conditions although the experimental trends are
254 quite well reproduced. Without CH_3NO_2 chemistry the model overpredicts the effect of adding
255 50 ppm NO and the simulation is unable to capture the $n\text{-C}_7\text{H}_{16}$ concentration profile for the 500
256 ppm NO case, particularly in the temperature window of 650-820 K. As in the case of methane
257 (Fig. 1), the CH_3NO_2 chemistry has a retarding effect in this temperature range. The model also
258 fails to predict the profiles of major species (CO, CO_2 , NO, and NO_2) in this temperature window
259 (650-820 K) when CH_3NO_2 chemistry is not included. In the presence of CH_3NO_2 chemistry, the
260 model prediction shows good agreement with the profiles of the major species, especially with
261 those of CO and CO_2 .

262 Furthermore, the simulation including the nitromethane sub-mechanism also affects the
263 predictions for intermediate species (for both 50 ppm and 500 ppm doped case), which closely
264 follow the experimental traces in terms of peak concentration, and breadth of temperatures as
265 shown in Fig. 6 and 7.

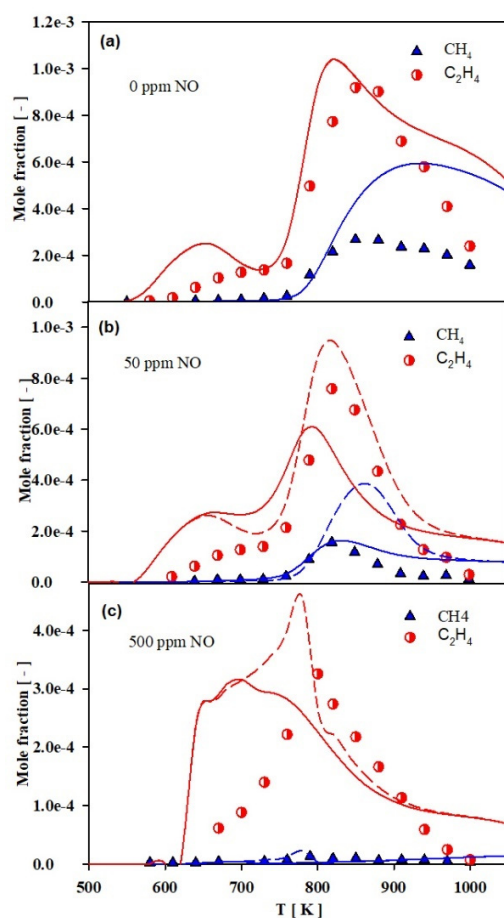
266



267

268 **Figure 6:** Oxidation of n-C₇H₁₆/O₂/N₂ in JSR doped with and without NO at 10 atm, $\phi = 1.0$, $\tau = 1.0$
 269 s. Symbols: measurements from [12], solid lines: prediction without CH₃NO₂ chemistry, dashed
 270 lines: prediction with CH₃NO₂ chemistry. Without NO in a mixture (a), with 50 ppm NO in a
 271 mixture (b, c).

272



273

274

275 **Figure 7:** Oxidation of $n\text{-C}_7\text{H}_{16}/\text{O}_2/\text{N}_2$ in JSR doped with and without NO at 10 atm, $\phi = 1.0$, $\tau = 1.0$
 276 s. Symbols: measurements from [11,12], solid lines: prediction without CH_3NO_2 chemistry,
 277 dashed lines: prediction with CH_3NO_2 chemistry. Without NO in a mixture (a), with 50 ppm NO in
 278 a mixture (b), with 500 ppm in a mixture (c).

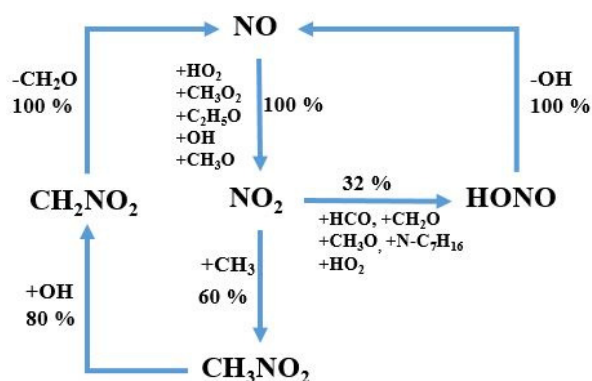
279 An integrated mass flux analysis (based on C-atoms for 500 ppm NO doped case) at 740 K
 280 reveals (see Fig. S7 in SM) that $n\text{-C}_7\text{H}_{16}$ mainly reacts to n -heptyl radicals *via* H atom abstraction
 281 by OH radicals. During the $n\text{-C}_7\text{H}_{16}$ degradation the CH_3 radical, which is crucial for the effect of
 282 CH_3NO_2 chemistry, is formed *via* the $\text{C}_2\text{H}_5 \rightarrow \text{C}_2\text{H}_5\text{O} \rightarrow \text{CH}_3$ route. The intermediate C_2H_5 reacts
 283 with NO_2 to form $\text{C}_2\text{H}_5\text{O}$ and NO ($\text{C}_2\text{H}_5 + \text{NO}_2 = \text{C}_2\text{H}_5\text{O} + \text{NO}$), the formed $\text{C}_2\text{H}_5\text{O}$ thermally
 284 dissociates to give $\text{CH}_3 + \text{CH}_2\text{O}$.

285 To elucidate the reaction pathways within the nitrogen chemistry (in 500 ppm NO doped case),
 286 we performed an integrated mass flux analysis based on N-atoms, from which the major paths
 287 are shown in Fig. 8. The analysis reveals that NO mainly reacts with HO_2 to give NO_2 in the reaction
 288 $\text{NO} + \text{HO}_2 = \text{NO}_2 + \text{OH}$. The minor channels that contribute to the formation of NO_2 are the direct

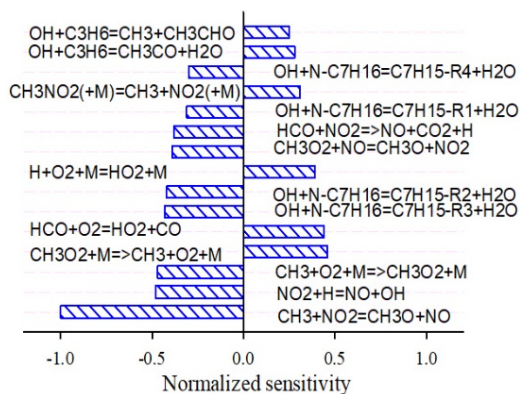
289 reaction of NO with CH_3O_2 ($\text{CH}_3\text{O}_2+\text{NO}=\text{CH}_3\text{O}+\text{NO}_2$), and the reverse reactions of
290 $\text{C}_2\text{H}_5+\text{NO}_2=\text{C}_2\text{H}_5\text{O}+\text{NO}$, $\text{NO}_2+\text{H}=\text{NO}+\text{OH}$, and $\text{CH}_3+\text{NO}_2=\text{CH}_3\text{O}+\text{NO}$. As in the case of CH_4 (Fig. 1),
291 NO_2 mainly goes to CH_3NO_2 (60 %) by recombining with CH_3 and 32 % of NO_2 goes to HONO
292 reacting with HCO , CH_2O , CH_3O , $n\text{-C}_7\text{H}_{16}$, and HO_2 . In line with the flow analysis, it can be seen in
293 Figure 5d that the model predicts the formation of significant amounts of CH_3NO_2 (black dashed
294 line). In the n -heptane case, CH_3NO_2 does not dissociate to $\text{CH}_3\text{O}+\text{NO}$ *via* the roaming mediated
295 channel but reacts *via* H atom abstraction, mainly by OH radicals, to CH_2NO_2 . The change in the
296 reaction path of CH_3NO_2 decomposition during n -heptane oxidation (Figure 8) is discussed below.
297 The formed CH_2NO_2 thermally dissociates to CH_2O and NO. The formed HONO undergoes thermal
298 decomposition to NO and OH recycling back NO and consequently producing more reactive OH
299 radicals. In the absence of CH_3NO_2 chemistry, its formation is promoted. All of the NO_2 will go to
300 HONO which will eventually thermally dissociate to NO and OH radicals *via* the same reaction
301 pathways discussed above. The predicted concentration profiles of HONO are a factor of 2 higher
302 without CH_3NO_2 chemistry (see Fig. S8 in the SM). It is clear from this analysis that for the system,
303 in which NO is present in the mixture, CH_3NO_2 acts like a sink for the NO_2 radical, which would
304 otherwise participate to produce more reactive OH radical accelerating the reactivity of the
305 system (see Fig. 5a). Furthermore, the model suggests that with CH_3NO_2 chemistry the formation
306 of the reactive radicals OH and HO_2 is delayed (moving towards higher temperature, see Fig. S8
307 in the SM), the same as seen for the methane case above (Fig. 4). The effect of CH_3NO_2 chemistry
308 on the overall reactivity is significant as can be seen in the sensitivity analysis (Fig. 9) which
309 identifies the recombination reaction $\text{CH}_3\text{NO}_2(+\text{M})=\text{CH}_3+\text{NO}_2(+\text{M})$ among the most sensitive
310 reactions at 740 K.

311 As stated above we observed a change in the reaction path of CH_3NO_2 decomposition during n -
312 heptane oxidation (Figure 8) compared to the CH_4 oxidation (Figure 2). The CH_3NO_2
313 decomposition is mainly controlled by OH and HO_2 formation. In the case of n -heptane oxidation
314 HO_2 begins to form at a much lower temperature compared to CH_4 (see Figure S10 in SM). The
315 higher amount of HO_2 formation at a lower temperature is due to the low temperature chemistry
316 (NTC regime) of n -heptane (the model reveals that many oxygenated species from n -heptane
317 chemistry contributes to HO_2 formation). However, CH_4 does exhibit low temperature chemistry
318 (NTC regime) and HO_2 formation is negligible compared to the n -heptane case (see Figure S10 in
319 SM). It is also interesting to observe that the formation of HO_2 and CH_3NO_2 begins at the same
320 temperature in the case of n -heptane oxidation. The early formation of HO_2 radicals in the case
321 of n -heptane oxidation supports the early formation of OH radical via route $\text{NO}+\text{HO}_2=\text{NO}_2+\text{OH}$
322 (80% of formed HO_2 is consumed to form OH). The formed OH radical reacts with CH_3NO_2 via the
323 H-abstraction channel to give CH_2NO_2 . In the case of CH_4 oxidation there is a lack of OH radicals
324 in the system at a lower temperature (see Figure S10 in SM). Furthermore, in the case of CH_4
325 oxidation (see Figure S10 in SM) at 900 K we observe the OH formation in the system. Indeed, at
326 this temperature model reveals that CH_3NO_2 reacts with OH radical to form CH_2NO_2

327 ($\text{CH}_3\text{NO}_2 + \text{OH} = \text{CH}_2\text{NO}_2 + \text{H}_2\text{O}$) and eventually leading to $\text{CH}_2\text{O} + \text{NO}$ via thermal dissociation of
 328 CH_2NO_2 (see Figure S11 in SM). This analysis leads to the conclusion that the decomposition path
 329 of CH_3NO_2 is mainly controlled by the radical pool in the system which can vary depending upon
 330 fuel and the system operating condition.



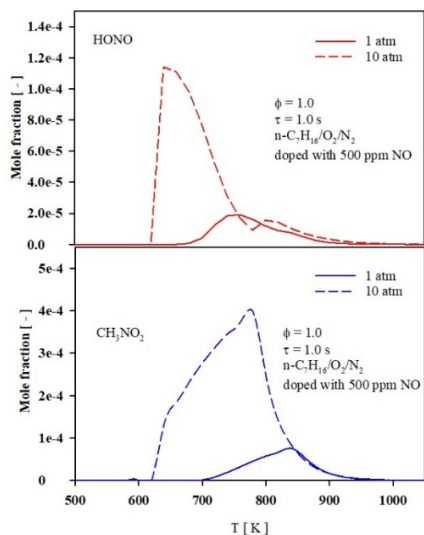
331
 332 **Figure 8:** Reaction path analysis based on N-atoms for the conditions shown in Figure 5 (here 500
 333 ppm of NO) at 740 K with CH_3NO_2 chemistry.



334
 335 **Figure 9:** Normalized sensitivity analysis for the conditions shown in Figure 5 (500 ppm of NO) at
 336 740 K towards $n\text{-C}_7\text{H}_{16}$.

337 Figure 10 illustrates the predicted mole fractions of the key intermediates HONO and CH_3NO_2
 338 during $n\text{-C}_7\text{H}_{16}/\text{O}_2/\text{N}_2$ oxidation in a JSR doped with 500 ppm of NO at 1 (solid lines) and 10 atm
 339 (dashed lines) respectively. It can be observed that a pressure increase from 1 to 10 atm,
 340 increases HONO and CH_3NO_2 concentrations by factors ~ 6 and 5 respectively. The stabilization of
 341 CH_3NO_2 at higher pressures supports HONO formation *via* CH_3NO_2 and reflects the pressure
 342 dependent $\text{CH}_3\text{NO}_2 (+\text{M}) = \text{CH}_3 + \text{NO}_2 (+\text{M})$ reaction. It should be noted that all the attempts to
 343 detect these two species in previous experimental studies [17,18] were carried out near 1 atm
 344 pressure. The findings of this work strongly suggest a high importance of CH_3NO_2 chemistry for

345 the ignition timing of *n*-heptane at elevated pressure (and engine relevant conditions), for which
346 an experimental detection of CH₃NO₂ and HONO may be possible.



347
348 **Figure 10:** Model predicted concentration profile comparison for HONO and CH₃NO₂ with CH₃NO₂
349 chemistry during oxidation of *n*-C₇H₁₆/O₂/N₂ in JSR doped with 500 ppm of NO, $\phi = 1.0$, $\tau = 1.0$ s
350 (a condition similar to Fig. 5). Solid lines: 1 atm, dashed lines: 10 atm.

351 4. Conclusion

352 A detailed investigation of the CH₃NO₂ chemistry effect on fuel-NO interactions has been
353 performed for the fuels methane and *n*-heptane using a recently developed and extensively
354 validated H₂/O₂/CO/NO_x/NH₃/CH₃NO₂ baseline chemistry. We found that CH₃NO₂ kinetics retard
355 the system reactivity in the low temperature range by delaying the production of key radicals like
356 OH and HO₂. This chemistry is crucial to understand and adequately simulate the delicate NO
357 effect on the ignition timing of *n*-heptane/NO mixtures, namely the transition from retardation
358 to reactivity enhancement at temperatures around 650 K. Further, the model suggests that
359 CH₃NO₂ is the major source of NO₂ consumption decreasing the concentration of HONO, which
360 is also formed *via* competing reactions of NO₂. For both fuels, HONO was found to contribute
361 significantly to the formation of OH and the recycling of NO. For *n*-heptane, the model suggests
362 that at higher pressure, relevant to engine condition, the two key intermediate species HONO
363 and CH₃NO₂ feature strongly increased concentrations and they may be detectable under high-
364 pressure conditions in combustion experiments of this fuel-NO_x system. The results of this work
365 call for detailed future investigations of the CH₃NO₂ chemistry effect in the context of exhaust
366 gas recirculation, also with regard to the suppression of engine knock. Clearly, the chemistry of
367 this key intermediate imposes important kinetic constraints for simulating the specific low-
368 temperature oxidation of fuel – NO_x systems.

369 **References**

- 370 [1] P.J. Crutzen, The role of NO and NO₂ in the chemistry of the troposphere and
371 stratosphere., *Annu. Rev. Earth Planet. Sci. Vol. 7*. 7 (1979) 443–472.
372 doi:10.1146/annurev.ea.07.050179.002303.
- 373 [2] K. Hoyer mann, F. Mauss, M. Olzmann, O. Welz, T. Zeuch, Exploring the chemical kinetics
374 of partially oxidized intermediates by combining experiments, theory, and kinetic
375 modeling, *Phys. Chem. Chem. Phys.* 19 (2017) 18128–18146. doi:10.1039/C7CP02759A.
- 376 [3] O. Welz, J.D. Savee, D.L. Osborn, S.S. Vasu, C.J. Percival, D.E. Shallcross, C.A. Taatjes,
377 Direct kinetic measurements of Criegee intermediate (CH₂OO) formed by reaction of CH₂I
378 with O₂., *Science*. 335 (2012) 204–7. doi:10.1126/science.1213229.
- 379 [4] L.V. Moskaleva, M.C. Lin, The spin-conserved reaction CH+N₂→H+NCN: A major pathway
380 to prompt no studied by quantum/statistical theory calculations and kinetic modeling of
381 rate constant, *Proc. Combust. Inst.* 28 (2000) 2393–2401. doi:10.1016/S0082-
382 0784(00)80652-9.
- 383 [5] W. Hack, M. Hold, K. Hoyer mann, J. Wehmeyer, T. Zeuch, Mechanism and rate of the
384 reaction CH₃+ O - Revisited, *Phys. Chem. Chem. Phys.* 7 (2005) 1977–1984.
385 doi:10.1039/b419137d.
- 386 [6] E. Goos, C. Sickfeld, F. Mauss, L. Seidel, B. Ruscic, A. Burcat, T. Zeuch, Prompt NO
387 formation in flames: The influence of NCN thermochemistry, *Proc. Combust. Inst.* 34
388 (2013) 657–666. doi:10.1016/j.proci.2012.06.128.
- 389 [7] J.M. Anderlohr, R. Bounaceur, A. Pires Da Cruz, F. Battin-Leclerc, Modeling of
390 autoignition and NO sensitization for the oxidation of IC engine surrogate fuels, *Combust.*
391 *Flame*. 156 (2009) 505–521. doi:10.1016/j.combustflame.2008.09.009.
- 392 [8] M. Sarabi, E. Abdi Aghdam, Experimental analysis of in-cylinder combustion
393 characteristics and exhaust gas emissions of gasoline–natural gas dual-fuel combinations
394 in a SI engine, *J. Therm. Anal. Calorim.* (2019) 1–14. doi:10.1007/s10973-019-08727-2.
- 395 [9] S.K. Prabhu, H. Li, D.L. Miller, N.P. Cernansky, The effect of nitric oxide on autoignition of
396 a primary reference fuel blend in a motored engine, in: *SAE Tech. Pap.* 932757, 1993.
397 doi:10.4271/932757.
- 398 [10] P. Dagaut, A. Nicolle, Experimental study and detailed kinetic modeling of the effect of
399 exhaust gas on fuel combustion: Mutual sensitization of the oxidation of nitric oxide and
400 methane over extended temperature and pressure ranges, *Combust. Flame*. 140 (2005)
401 161–171. doi:10.1016/j.combustflame.2004.11.003.

- 402 [11] G. Moréac, Experimental study and modelling of chemical interactions between gases
403 residual and fresh gas in the homogeneous spontaneous ignition gasoline engines, PhD
404 Thesis, University of Orléans, 2003. <https://tel.archives-ouvertes.fr/tel-02961685/>.
- 405 [12] G. Moréac, P. Dagaut, J.F. Roesler, M. Cathonnet, Nitric oxide interactions with
406 hydrocarbon oxidation in a jet-stirred reactor at 10 atm, *Combust. Flame.* 145 (2006)
407 512–520. doi:10.1016/j.combustflame.2006.01.002.
- 408 [13] R. Lan, J.T.S. Irvine, S. Tao, Ammonia and related chemicals as potential indirect
409 hydrogen storage materials, *Int. J. Hydrogen Energy.* 37 (2012) 1482–1494.
410 doi:10.1016/j.ijhydene.2011.10.004.
- 411 [14] K.P. Shrestha, L. Seidel, T. Zeuch, F. Mauss, Detailed Kinetic Mechanism for the Oxidation
412 of Ammonia Including the Formation and Reduction of Nitrogen Oxides, *Energy & Fuels.*
413 32 (2018) 10202–10217. doi:10.1021/acs.energyfuels.8b01056.
- 414 [15] K.P. Shrestha, L. Seidel, T. Zeuch, F. Mauss, Kinetic Modeling of NO_x Formation and
415 Consumption during Methanol and Ethanol Oxidation, *Combust. Sci. Technol.* 191 (2019)
416 1628–1660. doi:10.1080/00102202.2019.1606804.
- 417 [16] K.P. Shrestha, N. Vin, O. Herbinet, L. Seidel, F. Battin-Leclerc, T. Zeuch, F. Mauss, Insights
418 into nitromethane combustion from detailed kinetic modeling – Pyrolysis experiments in
419 jet-stirred and flow reactors, *Fuel.* 261 (2020) 116349. doi:10.1016/j.fuel.2019.116349.
- 420 [17] Y. Song, L. Marrodán, N. Vin, O. Herbinet, E. Assaf, C. Fittschen, A. Stagni, T. Faravelli,
421 M.U. Alzueta, F. Battin-Leclerc, The sensitizing effects of NO₂ and NO on methane low
422 temperature oxidation in a jet stirred reactor, *Proc. Combust. Inst.* 37 (2019) 667–675.
423 doi:10.1016/j.proci.2018.06.115.
- 424 [18] L. Marrodán, Y. Song, O. Herbinet, M.U. Alzueta, C. Fittschen, Y. Ju, F. Battin-Leclerc, First
425 detection of a key intermediate in the oxidation of fuel + NO systems: HONO, *Chem.*
426 *Phys. Lett.* 719 (2019) 22–26. doi:10.1016/j.cplett.2019.01.038.
- 427 [19] L. Seidel, K. Moshhammer, X. Wang, T. Zeuch, K. Kohse-Höinghaus, F. Mauss,
428 Comprehensive kinetic modeling and experimental study of a fuel-rich, premixed n-
429 heptane flame, *Combust. Flame.* 162 (2015) 2045–2058.
430 doi:10.1016/j.combustflame.2015.01.002.
- 431 [20] K.P. Shrestha, S. Eckart, A.M. Elbaz, B.R. Giri, C. Fritsche, L. Seidel, W.L. Roberts, H.
432 Krause, F. Mauss, A comprehensive kinetic model for dimethyl ether and
433 dimethoxymethane oxidation and NO_x interaction utilizing experimental laminar flame
434 speed measurements at elevated pressure and temperature, *Combust. Flame.* 218
435 (2020) 57–74. doi:10.1016/j.combustflame.2020.04.016.

- 436 [21] R.S. Zhu, M.C. Lin, CH₃NO₂ decomposition/isomerization mechanism and product
437 branching ratios: An ab initio chemical kinetic study, *Chem. Phys. Lett.* 478 (2009) 11–16.
438 doi:10.1016/J.CPLETT.2009.07.034.
- 439 [22] Z. Homayoon, J.M. Bowman, Quasiclassical trajectory study of CH₃NO₂ decomposition
440 via roaming mediated isomerization using a global potential energy surface, *J. Phys.*
441 *Chem. A.* 117 (2013) 11665–11672. doi:10.1021/jp312076z.
- 442 [23] R.S. Zhu, P. Raghunath, M.C. Lin, Effect of roaming transition states upon product
443 branching in the thermal decomposition of CH₃NO₂, *J. Phys. Chem. A.* 117 (2013) 7308–
444 7313. doi:10.1021/jp401148q.
- 445 [24] C.J. Annesley, J.B. Randazzo, S.J. Klippenstein, L.B. Harding, A.W. Jasper, Y. Georgievskii,
446 B. Ruscic, R.S. Tranter, Thermal Dissociation and Roaming Isomerization of
447 Nitromethane: Experiment and Theory, *J. Phys. Chem. A.* 119 (2015) 7872–7893.
448 doi:10.1021/acs.jpca.5b01563.
- 449 [25] A. Matsugi, H. Shiina, Thermal Decomposition of Nitromethane and Reaction between
450 CH₃ and NO₂, *J. Phys. Chem. A.* 121 (2017) 4218–4224. doi:10.1021/acs.jpca.7b03715.
- 451 [26] P.A. Vlasov, N.M. Kuznetsov, Y.P. Petrov, S. V. Turetskii, Nitromethane Isomerization
452 during Its Thermal Decay, *Kinet. Catal.* 59 (2018) 6–10.
453 doi:10.1134/S0023158418010147.
- 454 [27] <http://logesoft.com/logesoft-ware/>, (n.d.).
- 455 [28] H. Zhao, L. Wu, C. Patrick, Z. Zhang, Y. Rezgui, X. Yang, G. Wysocki, Y. Ju, Studies of low
456 temperature oxidation of n-pentane with nitric oxide addition in a jet stirred reactor,
457 *Combust. Flame.* 197 (2018) 78–87. doi:10.1016/j.combustflame.2018.07.014.
- 458 [29] Z. Chen, P. Zhang, Y. Yang, M.J. Brear, X. He, Z. Wang, Impact of nitric oxide (NO) on n-
459 heptane autoignition in a rapid compression machine, *Combust. Flame.* 186 (2017) 94–
460 104. doi:10.1016/j.combustflame.2017.07.036.
- 461 [30] P.A. Glaude, N. Marinov, Y. Koshiishi, N. Matsunaga, M. Hori, Kinetic modeling of the
462 mutual oxidation of NO and larger alkanes at low temperature, *Energy and Fuels.* 19
463 (2005) 1839–1849. doi:10.1021/ef050047b.
- 464 [31] A. Dubreuil, F. Foucher, C. Mounaïm-Rousselle, G. Dayma, P. Dagaut, HCCI combustion:
465 Effect of NO in EGR, *Proc. Combust. Inst.* 31 II (2007) 2879–2886.
466 doi:10.1016/j.proci.2006.07.168.
- 467